High-Precision Position Control of a Linear-Switched Reluctance Motor Using a Self-Tuning Regulator

Shi Wei Zhao, *Member, IEEE*, Norbert C. Cheung, *Senior Member, IEEE*, Wai-Chuen Gan, *Senior Member, IEEE*, and Jin Ming Yang

***Abstract*—High-precision position control of linear-switched reluctance motor (LSRM) is important in motion-control industry. The static model-based controller sometimes cannot give satisfactory output performance due to the inherent nonlinearities of LSRM and the uncertainties of the system. In this paper, a self-tuning regulator (STR) based on the pole-placement algorithm is proposed for high-precision position tracking of the LSRM. Following the time-scale characteristics analysis of LSRM position-tracking system and force-characteristic investigation, the position-tracking model is treated as a second-order system. Different from the static model-based control schemes, the dynamic model of the LSRM can be obtained by online estimation. Also, some practical aspects are taken into account. Owing to the unmodeled dynamics and high-frequency measurement noises, there are some oscillations in the practical control signals, and they can be reduced by a properly designed filter. Both the simulation and experimental results demonstrate that, in the control of the proposed STR, the position-tracking system can reproduce the reference signal with the desired performance in harsh ambient. These results confirm that the method is effective and robust in the high-precision position tracking of LSRM.**

***Index Terms*—Linear-switched reluctance motor (LSRM), motor-winding-excitation scheme, nonlinear characteristic, saturation, position control, self-tuning regulator (STR).**

I. Introduction

LINEAR-SWITCHED reluctance motor (LSRM) is an attractive candidate for the position and velocity control due to its low cost, simple structures, ruggedness and reliability in harsh environments, and capability of a wide speed range. Compared to the method of rotary motors with transformation components for producing linear motion, LSRM has many advantages, such as quick response, high sensitivity, and tracking capability; moreover, the structure of LSRM can reduce the room requirement for its installation. In addition, LSRM has a simpler and more rugged structure, and a lower system cost than direct-drive permanent-magnet linear-synchronous motor (PMLSM). These advantages make the LSRM as an alternative choice for the direct-drive applications. However, LSRM is difficult to be controlled and their outputs have high force ripples since the mathematical models of LSRM is highly dependent on their complex magnetic circuits that are difficult to be modeled, simulated, and controlled.

Several control methods and schemes have been proposed for the switched reluctance motors. General foundations for the practical design of a family of switched reluctance motors are explored in [1]; further, it demonstrates that the machines in this family provide the basis for fully controllable variable-speed system. In [2], a flux linkage-based controller is proposed for rotary-switched reluctance motor and experimental results show that low torque ripple can be achieved over a range of speed and torques. With considerations of nonlinear models, two feedback linearization controllers are designed for position and speed tracking of rotary-switched reluctance motor in [3] and [4]. Also, a proportional-integral (PI) controller is used to current control for LSRM in [5]. The aspects about speed control for LSRM are discussed in [6] and [7]. In [6], a PI controller is proposed for speed control. The auto-disturbance rejection controller is applied to speed control the LSRM in [7]. Precision-position control is reported in [8] and [9]. In [8], Gan *et al*. propose a simple yet effective position controller that uses a lookup table to linearize the relationship among phase force, current and position, and a plug-in compensator to improve the system robustness. A closed-form solution is further developed for short-distance position control in [9]. These control methods can be successfully implemented on LSRMs based on their static models. However, it may be necessary to adjust the controller parameters from time to time in the field to counteract the system uncertainties and external load disturbances.

Manufacturing imperfection for LSRM can result in the different characteristics during the mass production, such as the variation of the air gap, which would result in the variation of force generation. The parameters of the LSRM system often change with the operating conditions and time such as the frictional force of the linear-motion guide. For the precision-position control, moreover, the load disturbance and the saturation characteristics of drivers often result in the variation of the model parameters. In these cases, static models are hard to represent the real machine adequately during dynamic operating conditions. For high-performance LSRM drives, self-tuning regulator (STR) is a good choice to overcome the uncertainties. With online-system identification, the parameters of plant model can be obtained in real time. According to the certainty-equivalence principle, these parameters are treated as the true parameters and can be used to adjust the parameters of STR to achieve desired performance adaptively.

Manuscript received May 19, 2010; accepted May 21, 2010. Date of current version October 29, 2010. This work was supported by the University Grants Council under Project PolyU 5224/04E. Recommended for publication by Associate Editor A. Consoli.

S. W. Zhao and N. C. Cheung are with the Department of Electrical Engineering, The Hong Kong Polytechnic University, Kowloon, Hong Kong (e-mail: eencheun@inet.polyu.edu.hk; norbert.cheung@polyu.edu.hk).

W.-C. Gan is with the Motion Group, ASM Assembly Automation Hong Kong Ltd., Kwai Chung, Hong Kong (e-mail: wcgan@asmpt.com).

J. M. Yang is with the Electric Power College, South China University of Technology, Guangzhou, China (e-mail: jmyang@scut.edu.cn).

Digital Object Identifier 10.1109/TPEL.2010.2051685

TABLE I
ELECTRICAL AND MECHANICAL PARAMETERS OF THE LSRM

Pole width (Y_1)	6mm
Pole pitch (Y_2)	12mm
Phase width (X_1)	42mm
Phase separation (X_2)	10mm
Winding length (X_3)	18mm
Winding width (L)	25mm
Air gap width (Z)	0.5mm
Phase resistance	1.5Ω
Aligned inductance	10.2mH
Unaligned inductance	7.8mH
Mass of the moving platform (M)	1.8Kg
Friction constant (B)	0.08N*s*m^{-1}

In this paper, a control scheme of cascaded-dual loop is proposed. The inner loop is a current-control loop and the outer loop is a position-control loop. Because the control bandwidth of the current tracking is much quicker than that of the position-tracking loop in this system, the controlled plant, viewed from the outer loop, can be regarded as a second-order system and the current loop is treated as a proportional part. For a quick response of inner loop, a proportional controller with feedforward compensation is applied for the current tracking, and an STR based on pole-placement algorithm for the outer loop is designed to achieve high closed-loop performance. In addition, many practical aspects such as the external load disturbances, saturation characteristics, and measurement noise are taken into account in the STR scheme.

II. CONSTRUCTION AND MODELING OF LSRM

A. Configuration of LSRM

The design schematic of the LSRM system is shown in Fig. 1. A set of three-phase coils is installed on the moving platform as shown in Fig. 1. The three coils are of the same dimension. The body of the moving platform is manufactured with aluminum, so that the total weight of the moving platform and its inertia are low and the magnetic paths are decoupled. The stator track and the core of the windings are laminated with 0.5 mm silicon-steel plates. A 0.5-μm-resolution linear-optical encoder is integrated in the LSRM system to observe the motion profile of the moving platform and provide the feedback-position information. The electrical and mechanical parameters of the LSRM are listed in Table I.

B. Modeling of LSRM

The LSRM system has a highly nonlinear characteristic due to its nonlinear flux behavior. The fundamental equations of LSRM are the voltage balancing equation (1), the electromagnetic force production equation (2), and the mechanical movement equation (3). Here, v_j is the voltage applied to the terminals of phase *j*, i_j is the current of phase *j*, r_j is the winding resistance, and λ_j is the phase flux linkage of phase *j*, x is the displacement, f_e is the generated electromagnetic force, f_l is the external load force, and M and B are the mass and friction constant, respectively,

$$v_j = r_j i_j + \frac{d\lambda_j}{dt}, \qquad j = a, b, c \tag{1}$$

$$f_e = \sum_{j=a}^{c} \frac{\partial \int_0^{i_j} \lambda_j di_j}{\partial x} \tag{2}$$

$$f_e = M\frac{d^2x}{dt^2} + B\frac{dx}{dt} + f_l. \tag{3}$$

Based on the fact that the current-loop bandwidth is up to kilohertz while the output mechanical bandwidth is in the order of 10 Hz [8]; therefore, the two-time-scale analysis and design can be applied in the LSRM system. The dynamics of the mechanical position is much slower than that of the electrical current. When the mechanical variables are mainly discussed, the electromagnetic variables can be regarded as working in the steady states. The mechanical variables can be regarded as unchangeable while the electromagnetic variables are mainly discussed.

It is necessary to perform current commutation with position for a proper LSRM operation. Therefore, a motor-winding-excitation scheme is developed. Generally, a motor-winding-excitation scheme can be considered as a force distribution function (FDF) and an approximated function of inductance-change rate. The diagram of a motor-winding-excitation scheme can be represented as shown in Fig. 2. The FDF is used to compute the force for each phase according to the position and the direction. The approximated function of inductance-change rate is used to compute the phase current according to the command force of the phase and the position. Some methods have been proposed for the approximated function of inductance-change rate [5]–[10]. They can be classified into two types: the type of lookup table and the type of approximated function. If the FDF and the approximated function of inductance-change rate are chosen, the current can be calculated by the inverse function $f_j^{-1}(x, i_j)$ of the electromagnetic force production equation with command force and its position. As a result, the electromagnetic force production equation can be approximated as (4)

$$f_j(x, i_j) = \frac{1}{2}\frac{dL_j}{dx} i_j^2, \qquad j = a, b, c \tag{4}$$

where f_j is the generated electromagnetic force of phase *j* and dL_j/dx is the inductance-change rate of phase *j*.

In this paper, the FDF is chosen as in Table II [8] and the approximated function of inductance-change rate is described as in (5) [10]

$$\frac{dL_j(x_j(t))}{dx_j(t)} = -K_{pj}\sin\left(\frac{2\pi x_j(t)}{y_2}\right), \qquad j = a, b, c$$
$$x_b = x_a + \frac{2y_2}{3}$$
$$x_c = x_a + \frac{y_2}{3}. \tag{5}$$

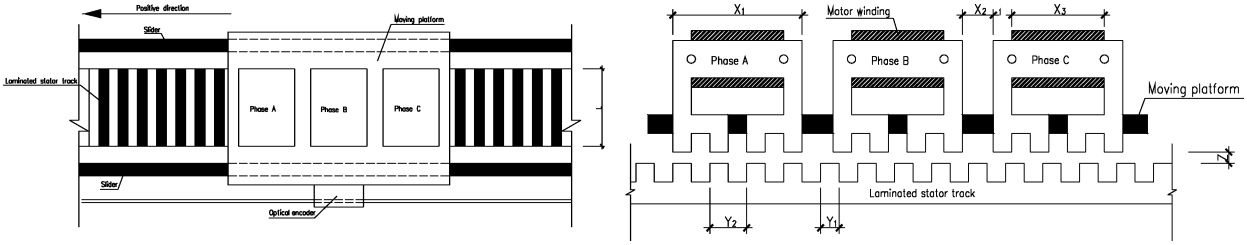

Fig. 1. Schematic of the LSRM.

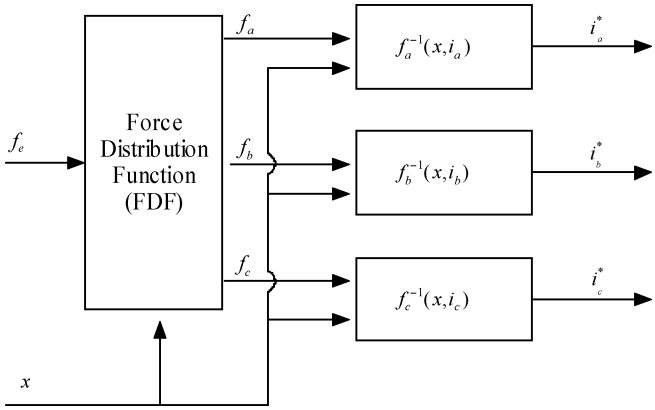

Fig. 2. Diagram of a motor-winding excitation scheme.

TABLE II
FORCE-DISTRIBUTION FUNCTION (FDF) SCHEME

Position range	+ force command	- force command
0mm-2mm	$f_B=f_x$	$f_C=0.5(2-x)f_x$, $f_A=0.5xf_x$
2mm-4mm	$f_B=0.5(4-x)f_x$, $f_C=0.5(x-2)f_x$	$f_A=f_x$
4mm-6mm	$f_C=f_x$	$f_A=0.5(6-x)f_x$, $f_B=0.5(x-4)f_x$
6mm-8mm	$f_C=0.5(8-x)f_x$, $f_A=0.5(x-6)f_x$	$f_B=f_x$
8mm-10mm	$f_A=f_x$	$f_B=0.5(10-x)f_x$, $f_C=0.5(x-8)f_x$
10mm-12mm	$f_A=0.5(12-x)f_x$, $f_B=0.5(x-10)f_x$	$f_C=f_x$

Here, y_2, x_j, and K_{pj} are the pole pitch of the LSRM, the displacement of phase j and a proportional parameter, respectively.

Using the approximated function of inductance-change rate in (5) and the FDF in Table II, the single phase and multiphase output-force experiment are performed on the proposed LSRM and the experimental data is shown in Fig. 3. The experimental figure of single phase shows the nonlinear force characteristics of the LSRM. From the experimental figure of multiphase, the output force is found to increase with the command force, but there are still some of the ripples in the force outputs. At the beginning, the output force increases quickly while the rate of output force gets slow with the increasing of the force command. In fact, the drivers of the LSRM system have got into the saturation region. The figures indicate that the output force is nonlinear to the position and force command. The parameters of the LSRM system, therefore, would change with its position and force command in operation.

In order to obtain the precise model in dynamic operation, online-parameter identification is applied. The parameters of the LSRM are online estimated by recursive least square (RLS) algorithm in this paper. As aforementioned, the LSRM can be considered as a second-order system from the outer loop when the dynamics of the currents are ignored. Define $y(t)$ as the output of a plant, $u(t)$ as the input of the plant, $w(t)$ as the disturbances, and q as the forward shift operator, the second-order system can be rewritten as the single-input, single-output discrete model given by (6)

$$A(q)y(t) = B(q)\{\mathrm{sat}[u(t),k] + w(t)\}, \qquad k > 0 \qquad (6)$$

where

$A(q) = q^2 + a_1 q + a_2$, $B(q) = b_0 q + b_1$ and

$$\mathrm{sat}[u(t),k] = \begin{cases} -k, u(t) < -k \\ u(t), |u(t)| \le k. \\ k, u(t) > k \end{cases}$$

For readability, the saturation function can be defined as

$$u_{\mathrm{sat}}(t,k) = \mathrm{sat}[u(t),k].$$

Then, (6) can be rewritten as

$$A(q)y(t) = B(q)[u_{\mathrm{sat}}(t,k) + w(t)].$$

III. SELF-TUNING REGULATOR DESIGN FOR LSRM

A. Parameter Identification of LSRM

The design of an STR is based on the online-parameter identification, which can represent the dynamics of the actual plant in real time. As aforementioned, the LSRM is assumed as a second-order system as (6). It can be seen that both of the load disturbances and the constraint of saturation contaminate the input signals and they can eventually result in the error of the estimation. Therefore, some filtering and pretreatment are required before the input and output signals are used for parameter identification. In order to avoid windup, the actual saturated input signals are fed back to the estimator. Usually, the load disturbance cannot be measured or used in estimation directly. However, it can be considered as relatively slow variable and can be diminished by a filter as follows [11]–[13]

$$\bar{u}(t) = \alpha\bar{u}(t-1) + u(t) - u(t-1)$$
$$\bar{y}(t) = \alpha\bar{y}(t-1) + y(t) - y(t-1), \quad 0 \le \alpha < 1$$

where $\bar{u}(t)$ and $\bar{y}(t)$ are the filtered input and output, respectively. α is a parameter of the filter. It could be chosen according to the actual requirements and performance.

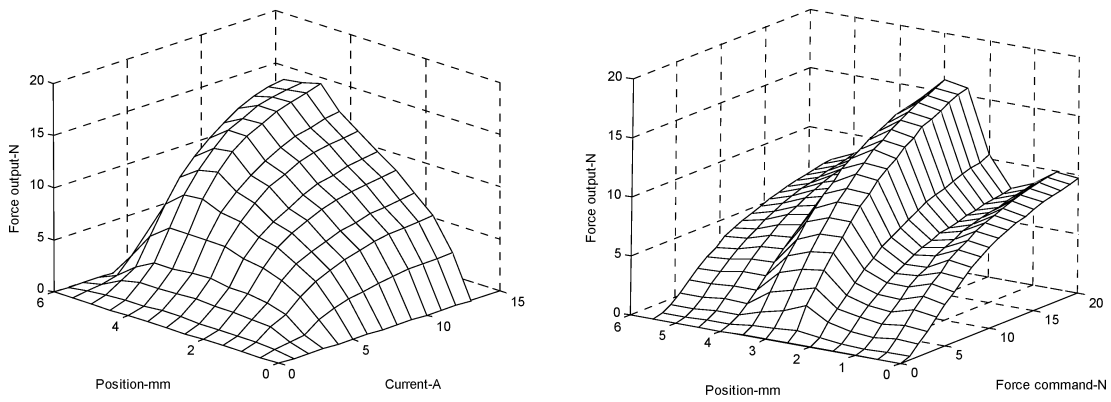

(a) (b)

Fig. 3. (a) Single-phase experimental current versus position versus force output 3-D chart and (b) multiphase experimental force command versus position versus force output 3-D chart.

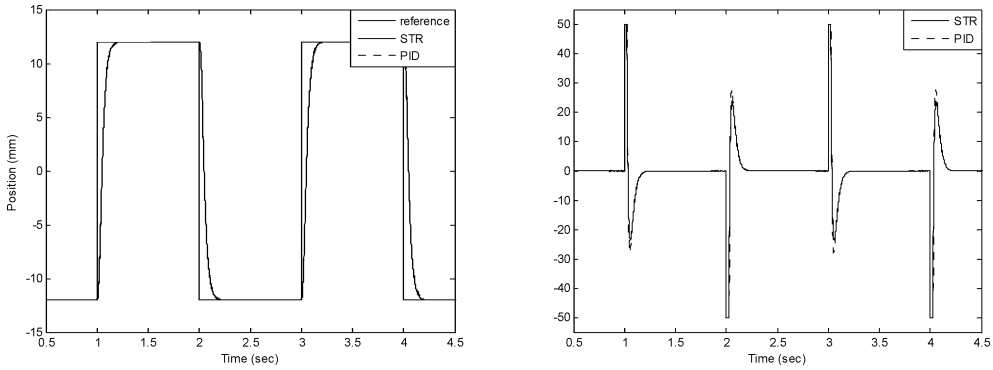

(a) (b)

Fig. 4. Simulation results of (a) trajectory response and (b) control signals of the LSRM system in the case of nominal state.

Therefore, the system model (6) can be rewritten as (7), which can be parameterized as (8)

$$A(q)\bar{y}(t) = B(q)\bar{u}_{\rm sat}(t,k) \tag{7}$$

$$\bar{y}(t) = \varphi^T(t-1)\theta(t-1) + \varepsilon(t) \tag{8}$$

where

$$\theta = [a_1, a_2, b_0, b_1]$$

$$\varphi^T(t-1) = [-\bar{y}(t-1), -\bar{y}(t-2), \bar{u}_{\rm sat}(t-1,k), \bar{u}_{\rm sat}(t-2,k)]$$

and $\varepsilon(t)$ is the residual.

Parameters of (8) can be estimated by the RLS algorithm [11] as

$$\theta(t) = \theta(t-1) + K(t)[\bar{y}(t) - \varphi^T(t)\theta(t-1)] \tag{9}$$

$$K(t) = P(t-1)\varphi(t)[\lambda + \varphi^T(t)P(t-1)\varphi(t)]^{-1} \tag{10}$$

$$P(t) = \frac{1}{\lambda}[I - K(t)\varphi^T(t)]P(t-1) \tag{11}$$

where P is the covariance matrix and λ is the forgetting factor. $K(t)$ can be interpreted as the adjusting gain. If $K(t) = 0$, then the estimated parameters θ converge to some constants. The forgetting factor λ, which can be given from 0 to 1, reflects the parameter-converging rate. If the forgetting factor is set at a small value, the estimated parameters would converge quickly with big ripples. On the other hand, when the forgetting factor is given a big value, the estimated parameters would converge slowly with small ripples. Here, the forgetting factor is given by 0.999. The initial covariance matrix $P(0)$ is selected as rI_4, which is a four-dimension unit matrix I_4 scaled by a positive scalar r, here r is given as a value of 10. And for the RLS algorithm, persistent excitation is required to make the estimated parameters to converge to their real values.

B. STR Design Based on the Pole-Placement Algorithm

In this paper, the STR is designed by the pole-placement algorithm. For a discrete plant, a general linear regulator can be described by (12)

$$R(q)u(t) = T(q)u_c(t) - S(q)y(t) \tag{12}$$

where $R(q)$, $S(q)$, and $T(q)$ are polynomials, $u_c(t)$ is the reference signal, and $R(q)$ is assumed to be a monic polynomial. To obtain a causal regulator in the discrete time case, the following conditions must be imposed: $\deg S \leq \deg R$ and $\deg T \leq \deg R$ [11]. By defining the desired-pole polynomial as $A_m(q)$, the closed-loop pole equation can be presented as

$$A(q)R(q) + B(q)S(q) = A_0(q)A_m(q) \tag{13}$$

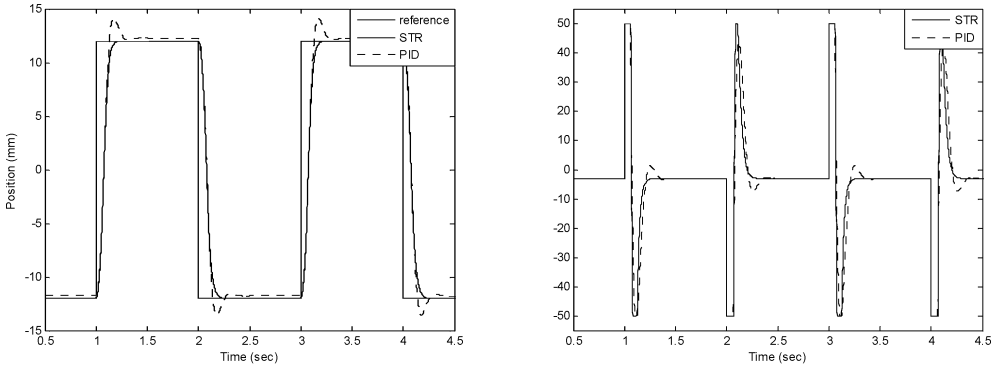

(a) (b)

Fig. 5. Simulation results of (a) trajectory response and (b) control signals of the LSRM system in the case of 150% mass increase, 70% system gain, and an external load disturbance.

where $A_0(q)$ is referred as the observer polynomial, which is a stable polynomial and can be canceled by zeros and the $T(q)$ can be chosen as

$$T(q) = \beta A_0(q) \tag{14}$$

where $\beta = A_m(1)/B(1)$. The closed-loop equation of the control system can be obtained as (15) by combining (6) with (12)

$$y(t) = \frac{B(q)T(q)}{A(q)R(q) + B(q)S(q)}u_c(t) + \frac{B(q)R(q)}{A(q)R(q) + B(q)S(q)}w(t). \tag{15}$$

From the closed-loop equation, the output is decided by the reference signal and the disturbances. For reproducing the reference signal as accurately as possible, the polynomial gain corresponding to the disturbances can be set as zero. In many cases, the disturbances are relatively slow to the reference signals. A factor of $(q-1)$, therefore, should be included in $R(q)$. This clearly gives integral action as commonly employed in practical control system design. At last, the saturation characteristic of actuators should be considered in the controller design. The saturation effect of actuators may create difficulties, especially if the controller has integral action. In this case, the control signal can be calculated by the following modified algorithm [11], [12] and [14], [15]

$$u_{\rm sat}(t,k) = \text{sat}\{T^*(q^{-1})u_c(t) - S^*(q^{-1})y(t) + [1 - R^*(q^{-1})]u_{\rm sat}(t,k), k\} \tag{16}$$

where $R^*(q^{-1})$, $S^*(q^{-1})$, and $T^*(q^{-1})$ are polynomials of $R(q)$, $S(q)$, and $T(q)$ in (12) in the style of delay operator, respectively.

IV. Simulation Results

In this section, the performance of the proposed STR is illustrated. The simulation results are achieved with the MATLAB software package. The parameter values of the LSRM system employed in the simulations are listed in Table I. In some industrial applications, the performance of overshoot free is required. In the simulations, the parameters of the reference model are

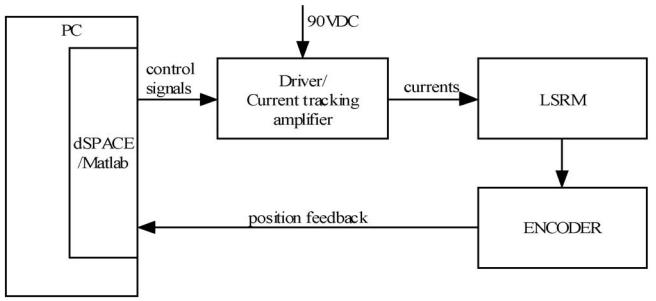

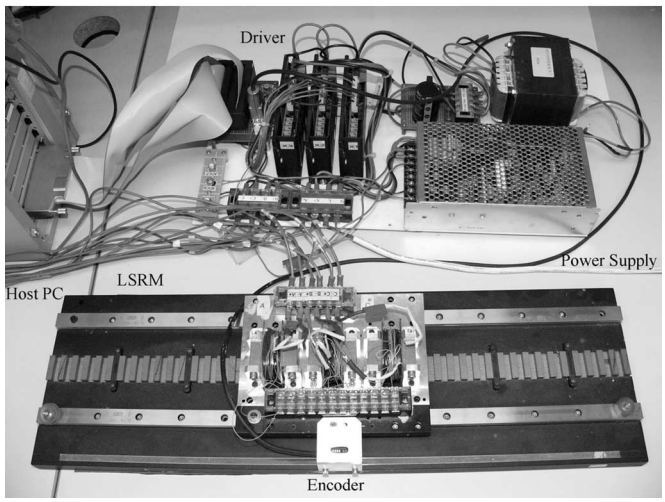

Fig. 6. Experimental setup.

chosen as $a_{1m} = -1.912$ and $a_{2m} = 0.9139$, the observer polynomial is chosen as $(q-0.5)(q-0.5)$ and the sampling time is set to 0.001 s. This parameter selection can make the LSRM system overshoot free. Fig. 4 shows a simulation comparison of output waveforms and control signals between the STR and a conventional proportional–integral–derivative (PID) control in the nominal state. It can be seen that both of the two control schemes are with good tracking ability and can reproduce the reference signal accurately. However, in the presence of parameter variation and disturbances the results are quite different. For example, the LSRM is operated in a different state from the

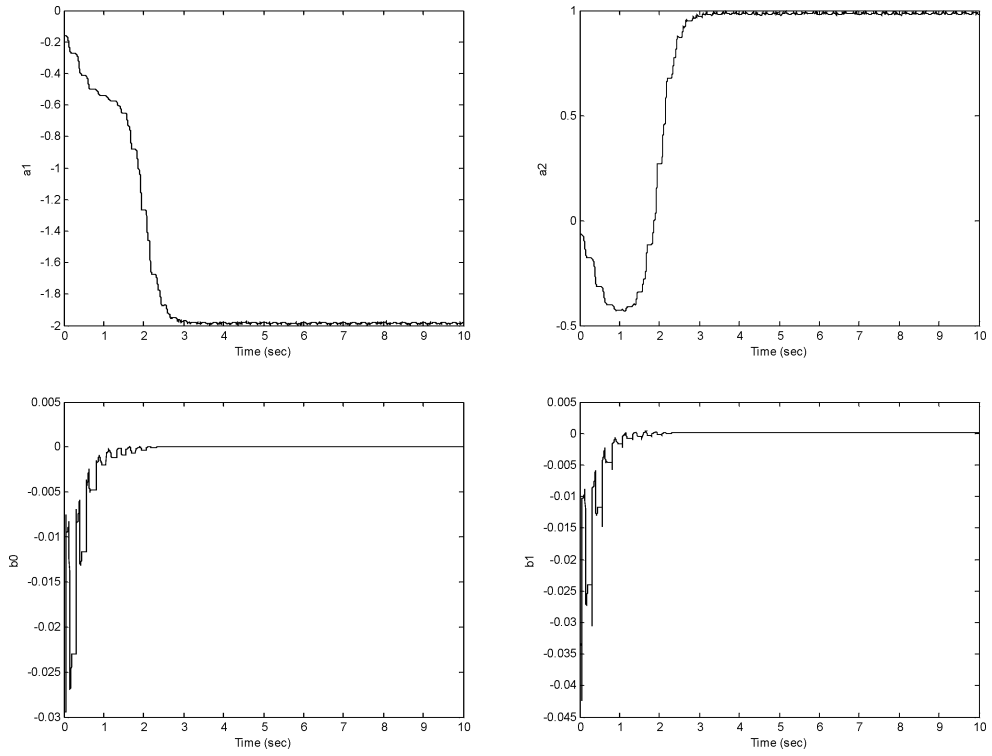

Fig. 7. Parameters estimation of the LSRM.

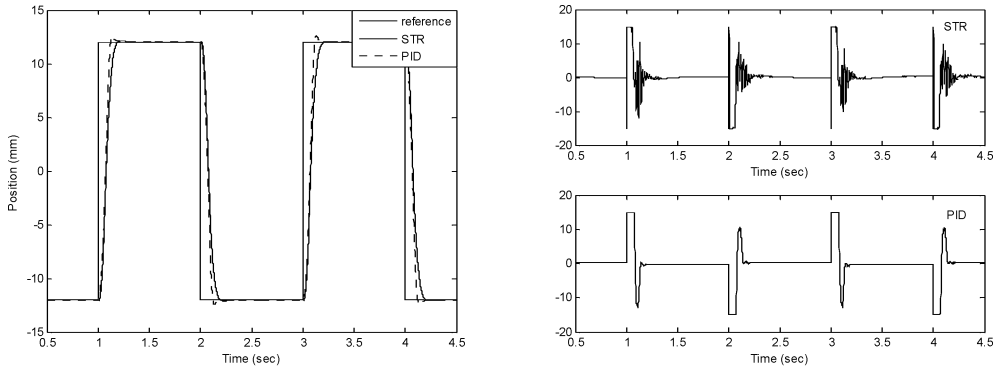

(a) (b)

Fig. 8. (a) Position-tracking waveforms and (b) control signals of the LSRM system in the case of nominal state.

nominal state. Compared with the nominal state, the mass of the moving platform is increased to 150%, the open-loop gain is reduced drastically to 50%, and an external load disturbance is applied to the model of LSRM. Its simulation results correspondingly are shown in Fig. 5. From the figures, the differences of the outputs under the two control schemes are obvious. The output under the STR control is the same as that of the nominal state, but the output under the PID control is deteriorated.

V. Experimental Implementation Results

The experimental setup is shown in Fig. 6. The host PC is a Pentium 4 computer that is used to download the target code into a dSPACE DS1104 DSP motion controller card. The control algorithm is developed under the environment of MATLAB/SIMULINK. All control functions are implemented by the DS1104 card, which is plugged into a peripheral component interconnect (PCI) bus of the host PC. For the current-tracking amplifier, the driver consists of three asymmetric bridge insulated gate bipolar transistor inverters with 90 V_{dc} voltage supplier. A linear-optical encoder with 0.5 μm resolution is mounted on the mover of the LSRM system and provides position feedback information. In the experiment, the control signal is the sum of the weighted proportional–derivative (PD) control signal and STR signal. At the beginning, the LSRM is operated by the PD controller. Then the control signal is switched on continuously a few seconds later. Finally, the LSRM is fully operated by the STR. Because of lack of the prior knowledge about the plant, a displacement impact for the LSRM would be resulted if the STR is fully switched on at the beginning of the

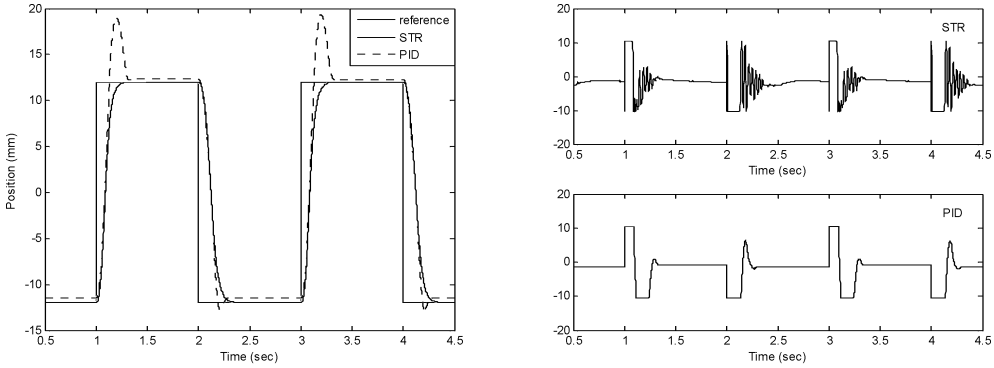

Fig. 9. (a) Position-tracking waveforms and (b) control-output waveforms with the 150% mass increase, 70% system gain, and an external load disturbance.

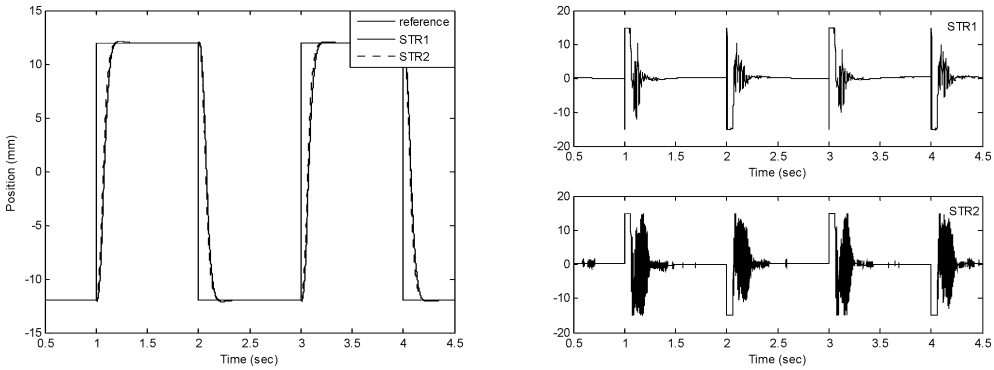

Fig. 10. (a) Position-tracking waveforms and (b) control signals with different observer polynomials. The upper figure of (b) is with poles far from original point and the bottom figure is with poles near original point.

operation. However, the weighted control method can avoid the impact of motor at the beginning of the operation.

In the experiment, the LSRM system is considered as a second-order system (6) with the sampling time 0.001 s and (7) is used as the parameter-estimation model. The estimation results for the proposed LSRM system are shown in Fig. 7. From the figures, the parameters converge to their stable values quickly. The parameters get their stable values at 2.5 s.

In the case of the nominal state, the position-tracking profiles and their corresponding control signals under the control of the proposed STR and a conventional PID controller are given in Fig. 8. It can be seen that both of the two controllers can achieve accurate position tracking with good dynamic performances. As a comparison, Fig. 9 shows the corresponding experimental results with the different parameters. In this case, the mass of the moving platform is increased to 150%, the open-loop gain is reduced drastically to 70%, and an external load disturbance is applied to the LSRM. The experimental results are similar to the simulation results. From the figures, the outputs under the PID controller are with different dynamic performance in the case of the parameter variation and the presence of disturbances. The overshoot of the output waveform for the PID controller gets obvious when the open-loop gain is reduced and the mass of moving platform is increased. In the presence of disturbances, there is a small steady error in the output. However, the outputs using the STR can track the reference signal with the desired performance in these cases.

From the earlier figures, a few of the oscillations exist in the STR-control signals. Too many oscillations would result in large power consumption, switch loss, and some ripples in the system output. Since practical environment is different from that of the simulation, there are many high-frequency noises and some of unmodeled dynamics such as static frictions, etc. These factors would act on the system and eventually result in some differences from the simulations. In fact, it can be found that the degree of oscillations is different with the observer polynomials as shown in Fig. 10, although the outputs for both control signals are similar. As shown in the bottom figure of Fig. 10(b), the oscillations are obvious when the zeros of observers are chosen nearby the origin. The oscillations, therefore, would be greatly reduced by choosing the zeros of observers far from the origin as shown in the upper figure of Fig. 10(b).

VI. Conclusion

In this paper, an STR based on the pole-placement algorithm has been proposed for high-precision position tracking of the LSRM. Following the time-scale characteristics analysis of LSRM position-tracking system and force characteristic investigation, the position-tracking model is treated as a second-order

system. Different from the static model-based control schemes, the dynamic model of the LSRM can be obtained by online estimation. Also, some practical aspects are taken into account. Owing to the unmodeled dynamics and high-frequency measurement noises, there are some oscillations in the practical control signals, and they can be reduced by a properly designed filter. Both the simulation and experimental results demonstrate that, in the control of the proposed STR, the position tracking of the LSRM can reproduce the reference signal with the desired performance in the case of harsh ambient such as the changes of system parameters, external load disturbances, and saturation of the drivers. These results confirm that the method is effective and robust in the high-precision position tracking of the LSRM.

ACKNOWLEDGMENT

The authors would like to thank for the general support of South China University of Technology through National Natural Science Foundation of China under Grant 60674099.

REFERENCES

[1] P. J. Lawrenson, J. M. Stephenson, P. T. Blenkinsop, J. Corda, and N. N. Fulton, "Variable-speed switched reluctance motors," *Inst. Elect. Eng. Pro.-Electr. Power Appl.*, vol. 127, Pt. B, no. 4, pp. 253–265, Jul. 1980.

[2] P. G. Barrass and B. C. Mecrow, "Flux and torque control of switched reluctance machines," *Inst. Elect. Eng. Pro.-Electr. Power Appl.*, vol. 145, no. 6, pp. 519–527, Nov. 1998.

[3] M. Ilic'-Spong, R. Marino, S. M. Peresada, and D. G. Taylor, "Feedback linearizing control of switched reluctance motors," *IEEE Trans. Automat. Control*, vol. AC-32, no. 5, pp. 371–379, May 1987.

[4] S. K. Panda and P. K. Dash, "Application of nonlinear control to switched reluctance motors: A feedback linearization approach," *Inst. Elect. Eng. Pro.-Electr. Power Appl.*, vol. 143, pp. 371–379, Sep. 1996.

[5] H. K. Bae, B. S. Lee, P. Vijayraghavan, and R. Krishnan, "A linear switched reluctance motor: Converter and control," *IEEE Trans. Ind. Appl.*, vol. 36, no. 5, pp. 1351–1359, Sep./Oct. 2000.

[6] J. L. Dorningos, D. A. Andrade, M. A. A. Freitas, and H. De Paula, "A new drive strategy for a linear switched reluctance motor," in *Proc. Electr. Mach. Drives Conf.*, Jun. 2003, vol. 3, pp. 1714–1719.

[7] J. F. Pan, S. C. Kwok, N. C. Cheung, and J. M. Yang, "Auto disturbance rejection speed control of linear switched reluctance motor," in *Proc. Ind. Appl. Conf.*, Oct. 2005, vol. 4, pp. 2491–249.

[8] W. C. Gan, N. C. Cheung, and L. Qiu, "Position control of linear switched reluctance motors for high precision applications," *IEEE Trans. Ind. Appl.*, vol. 39, no. 5, pp. 1350–1362, Sep./Oct. 2003.

[9] W. C. Gan, N. C. Cheung, and L. Qiu, "Short distance position control for linear switched reluctance motors: A plug-in robust compensator approach," in *Proc. IEEE Ind. Appl. Conf.*, Sep./Oct. 2001, vol. 4, pp. 2329–2336.

[10] F. Khorrami, P. Krishnamurthy, and H. Melkote, *Modeling and Adaptive Nonlinear Control of Electric Motors*. New York: Springer-Verlag, 2003.

[11] K. J. Åström and B. Wittenmark, *Adaptive Control*. Reading, MA: Addison-Wesley, 1995.

[12] I. D. Landau, *System Identification and Control Design*. Englewood Cliffs, NJ: Prentice-Hall, 1990.

[13] S. S. Wilson and C. L. Carnal, "System identification with disturbances," in *Proc. 26th Southeastern Symp. Syst. Theory*, Mar. 1994, pp. 502–506.

[14] D. Y. Abramovitch and G. F. Franklin, "On the stability of adaptive pole-placement controllers with a saturating actuator," *IEEE Trans. Automat. Control*, vol. 35, no. 3, pp. 303–306, Mar. 1990.

[15] G. C. Goodwin and K. S. Sin, *Adaptive Filtering Prediction and Control*. Englewood Cliffs, NJ: Prentice-Hall, 1984.

Shi Wei Zhao (S'07–M'09) received the B.Sc. degree from the Central South University, Changsha, China, the M.Sc. degree from the South China University of Technology, Guangzhou, China, and the Ph.D. degree from The Hong Kong Polytechnic University, Kowloon, Hong Kong, in 2000, 2003, and 2008, respectively.

He is currently a Postdoctoral Fellow in the Department of Electrical Engineering, The Hong Kong Polytechnic University. His research interests include motion control and machine drives.

Norbert C. Cheung (S'85–M'91–SM'05) received the B.Sc. degree from the University of London, London, U.K., the M.Sc. degree from the University of Hong Kong, Pokfulam, Hong Kong, and the Ph.D. degree from the University of New South Wales, Kensington N.S.W., Australia, in 1981, 1987, and 1995, respectively.

He is currently in the Department of Electrical Engineering, The Hong Kong Polytechnic University, Kowloon, Hong Kong. His research interests include motion control, actuators design, and power electronic drives.

Wai-Chuen Gan (S'94–M'02–SM'06) received the B.Eng. degree (with first-class honors) in electronic engineering, and the M.Phil. and Ph.D. degrees in electrical and electronic engineering from the Hong Kong University of Science and Technology, Hong Kong, China, in 1995, 1997, and 2001, respectively.

From 1997 to 1999, he was a Motion Control Application Engineer at ASM Assembly Automaton Ltd., Hong Kong, China. He rejoined the ASM Assembly Automaton Ltd. in 2002, where he is currently involved in the development of linear-switched reluctance motor systems for semiconductor-assembly equipment. His research interests include robust control of ac machines, power electronics, design and control of the linear-switched reluctance motors.

Dr. Gan is the recipient of the Academic Achievement Award.

Jin Ming Yang received the B.Sc. degree from the University of Beijing Aeronautics, Beijing, China, the M.Sc. degree from the Zhejiang University, Hangzhou, China, and the Ph.D. degree from the South China University of Technology, Guangzhou, China, in 1987, 1990, and 2000, respectively.

He is currently an Associate Professor at the South China University of Technology. His research interests include machine drives and nonlinear control.